



Sustainable and Biodegradable Wood Sponge Piezoelectric Nanogenerator for Sensing and Energy Harvesting Applications

Journal Article

Author(s):

Sun, Jianguo; Guo, Hengyu; Ribera, Javier; Wu, Changsheng; [Tu, Kunkun](#) ; Binelli, Marco; [Panzarasa, Guido](#) ; Schwarze, Francis W.M.R.; Wang, Zhong Lin; Burgert, Ingo

Publication date:

2020-11-24

Permanent link:

<https://doi.org/10.3929/ethz-b-000453242>

Rights / license:

[In Copyright - Non-Commercial Use Permitted](#)

Originally published in:

ACS Nano 14(11), <https://doi.org/10.1021/acsnano.0c05493>

A Sustainable and Biodegradable Wood Sponge

Piezoelectric Nanogenerator for Sensing and

Energy Harvesting Applications

*Jianguo Sun[†], Hengyu Guo[‡], Javier Ribera[Ⓔ], Changsheng Wu[‡], Kunkun Tu[†], Marco Binelli[#],
Guido Panzarasa[†], Francis W.M.R. Schwarze[Ⓔ], Zhong Lin Wang^{‡,*}, Ingo Burgert^{†,*}*

[†]Wood Materials Science, Institute for Building Materials, ETH Zürich, 8093, Switzerland,

[‡]School of Materials Science and Engineering, Georgia Institute of Technology, Atlanta, GA
30332

[Ⓔ]Laboratory for Cellulose & Wood Materials, Empa, Lerchenfeldstrasse 5, 9014, Switzerland.

[#]Complex Materials, Department of Materials, ETH Zürich, 8093, Switzerland.

*Corresponding authors. E-mail: iburgert@ethz.ch (I.B.), zhong.wang@mse.gatech.edu
(Z.L.W.)

ABSTRACT

Developing low-cost and biodegradable piezoelectric nanogenerators is of great importance for a variety of applications, from harvesting low-grade mechanical energy to wearable sensors. Many of the most widely used piezoelectric materials, including lead zirconate titanate (PZT), suffer from serious drawbacks such as complicated synthesis, poor mechanical properties (*e.g.* brittleness) and toxic composition, limiting their development for biomedical applications and posing environmental problems for their disposal. Here, we report a low-cost, biodegradable, biocompatible and highly compressible piezoelectric nanogenerator based on a wood sponge obtained with a simple delignification process. Thanks to the enhanced compressibility of the wood sponge, our wood nanogenerator ($15 \times 15 \times 14 \text{ mm}^3$, longitudinal \times radial \times tangential) can generate an output voltage of up to 0.69 V, 85 times higher than that generated by native (untreated) wood, and it shows stable performance under repeated cyclic compression (≥ 600 cycles). Our approach suggests the importance of increased compressibility of bulk materials for improving their piezoelectric output. We demonstrate the versatility of our nanogenerator by showing its application both as a wearable movement monitoring system (made with a single wood sponge) and as a large-scale prototype with increased output (made with 30 wood sponges) able to power simple electronic devices (a LED light, a LCD screen). Moreover, we demonstrate the biodegradability of our wood sponge piezoelectric nanogenerator by studying its decomposition with cellulose-degrading fungi. Our results showcase the potential application of wood sponge as a sustainable energy source, as a wearable device for monitoring human motions, and its contribution to environmental sustainability by electronic waste reduction.

KEYWORDS: wood sponge, piezoelectric nanogenerator, biocompatible and biodegradable, energy source, pressure sensor

Increased depletion of fossil fuels and severe environmental pollution have motivated considerable efforts to find alternative and more sustainable energy sources.¹⁻³ During the past decades many renewable and clean energy sources have been developed, including wind and solar energy. However, these latter are highly dependent on weather and other environmental conditions.⁴⁻⁶ Mechanical energy exists ubiquitously in various forms, including sound waves and human movements, and does not suffer limitations from bad weather.^{7, 8} Mechanical energy can be harvested from the surrounding environment by means of electromagnetic,⁹ piezoelectric^{10, 11} and triboelectric generators.¹²⁻¹⁸ Piezoelectric nanogenerators, in particular, have triggered intensive research.^{19, 20} Many materials have been utilized to fabricate piezoelectric nanogenerators, including nanostructures made of zinc oxide ZnO, lead zirconate titanate $\text{Pb}[\text{Zr}_x\text{Ti}_{1-x}]\text{O}_3$ ($0 \leq x \leq 1$, PZT) and barium titanate BaTiO_3 , or polymers such as poly(vinylidene fluoride) (PVDF) and its copolymers based on trifluoroethylene [P(VDF-TrFE)].²¹⁻²³ However, most of these materials, such as PZT, are brittle ceramics that contain toxic elements (lead), which limits their use for wearable and biomedical applications,²¹ or are non-biodegradable, like PVDF and [P(VDF-TrFE)].²¹⁻²³ As a result, these materials could cause serious ecological damage as a result of improper disposal after their life cycle.²⁴ Thus, there is great interest in developing piezoelectric generators made of biocompatible, renewable and biodegradable materials, assembled with environmentally friendly technologies.

Wood is one of the most abundant natural resources on Earth, and it is renewable, lightweight, biocompatible and biodegradable. Wood cell walls are mainly composed of cellulose (organized in amorphous and crystalline regions), hemicelluloses, and lignin.²⁵ Thanks to the uniaxial orientation and monoclinic symmetry of crystalline cellulose fibrils, wood does behave as a piezoelectric material.²⁵⁻²⁷ However, due to the low piezoelectric constant (previously reported it to be approx. 1/20 of that of quartz)²⁶ and poor deformability of natural

wood, limited progress has been made in the past decades for its application in piezoelectric devices.²⁷ As cellulose crystals are framed in wood,²⁸ increasing the dynamic deformability of macroscopic wood, making the displacement of cellulose crystal easier under a minute load, should result in a dramatic efficiency increase of piezoelectricity generation in wood.

Here we report a low-cost, biodegradable, biocompatible and highly compressible piezoelectric nanogenerator fabricated from delignified balsa wood. By removal of lignin and hemicellulose with a simple and fast chemical treatment, balsa wood was transformed into highly compressible wood sponges, resulting in an increment of the electrical output of over 85 times compared to native wood.²⁹⁻³¹ Moreover, our wood sponge can generate electricity without the need of any electrical poling (a process that forces the dipoles to orient themselves in a prescribed direction, enhancing the piezoelectric effect.³²). Compared to previously reported wood- or cellulose-based triboelectric or piezoelectric nanogenerators, the wood sponge can generate effective electrical output without the need of inserting additional chemical materials, making it more sustainable and suitable for biomedical applications.^{33, 34} Our top-down approach allows us to take advantage of wood's bulk structure, and requires less process steps compared to more commonly exploited approaches based on disassembly of wood and subsequent composition in bottom-up processes.³⁵ Our wood sponge piezoelectric nanogenerator can be attached on a rugged skin to monitor human motions, thanks to the electrical signals generated in response to different applied mechanical stresses. Pressing with the finger or tapping with the foot on this prototype generated enough current to power a commercial LED or LCD screen, suggesting its efficiency as energy source. Moreover, the wood sponges are biodegradable, which demonstrates that it is possible to produce recyclable piezoelectric nanogenerators from wood, a renewable CO₂-neutral material.

RESULTS AND DISCUSSION

Natural wood is not an ideal piezoelectric material due to its relatively low compressibility. However, this characteristic can be enhanced by the selective removal of lignin. As one of the lightest woods, balsa (*Ochroma pyramidale*) was selected as starting material since its thin cell walls facilitate the delignification process.³⁶ As illustrated schematically in Figure 1(a), wood has a honeycomb-like structure that is modified into a spring-like lamellar structure *via* a one-step chemical delignification based on a concentrated mixture of hydrogen peroxide and acetic acid, followed by a freeze-drying step. Hydrogen peroxide, a relatively stable and mild oxidant, can be regarded as the ultimate “green” reagent, water and oxygen being its only by-products.³⁷ Acetic acid is an excellent alternative to mineral acids. The acid waste produced can be easily neutralized by the addition of base, generating harmless acetate salts that could be recycled. For these reasons, the process could be considered as sustainable. After the selective removal of lignin and hemicellulose, the resulting structure can support repeated compression without structural failure. Upon compression, the wood sponge generates charges, that can be collected on its surface, thanks to the intrinsic piezoelectric behavior of crystalline cellulose. Higher compressibility results in larger displacement of crystalline cellulose, enhancing the electrical output.

Figure 1(b) and (c) compare balsa wood before and after the chemical delignification treatment. The native balsa wood has a yellowish color while the wood sponge after chemical treatment is white, indicating removal of a greater part of lignin. Compared to native wood, the wood sponge shows a shrinkage in size along the tangential direction. More detailed changes in morphology and microstructure were observed by scanning electron microscopy (SEM). After delignification, the honeycomb-like wood structure was changed into lamellar structure with many stacked arched layers. (Figure 1(b), (c) and S1) In addition, high-resolution SEM images revealed that after removal of lignin and hemicellulose, the original

compact cell walls were detached and cell lumina coalesced into large voids. Delignification of the balsa wood was further confirmed by Fourier transform-infrared (FT-IR) analysis, where the characteristic peaks of lignin at 1594, 1505, and 1457 cm^{-1} vanished after the chemical treatment (Figure 1(d)).²⁹ The peaks at 1735 cm^{-1} and 1238 cm^{-1} showed a shifting and decrease in the relative intensities, indicating partial removal of hemicellulose.³¹

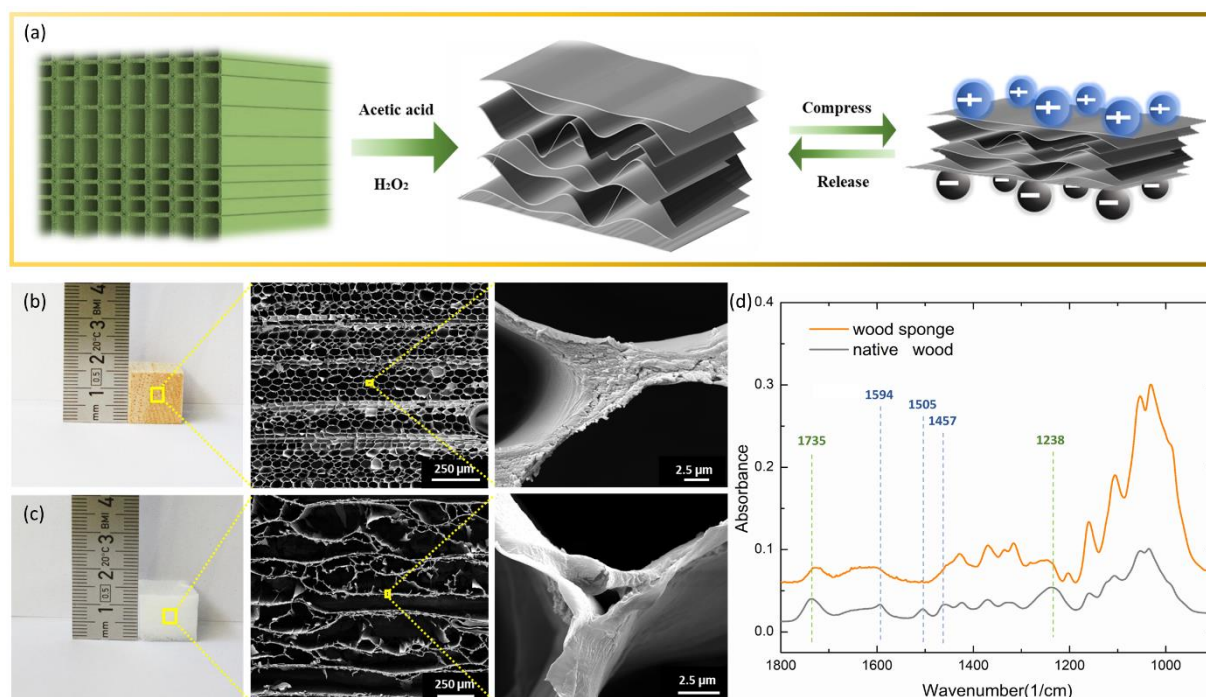


Figure 1. (a) Schematic illustration of the fabrication steps of wood sponges from native balsa wood and its piezoelectric behavior. The pictures of (b) native balsa wood and (c) the resulting wood sponge are shown along with the scanning electron microscopy (SEM) images of their transverse sections to illustrate the morphological changes introduced by the delignification process. (d) Comparison between the FT-IR spectra of native balsa wood and of the resulting wood sponge.

Further changes in the morphology and structure of balsa wood *via* chemical treatment over time up to 48 h were observed by performing SEM on transverse sections. As shown in Figure 2(a) and S2, the native wood possesses a honeycomb-like porous structure with thin cell walls. The diameter of the cell lumina varied from 20 to 50 μm . After 3 h of chemical treatment, the structure changed only slightly (Figure 2(b)). Some cracks were observed after 6 h, when longitudinally oriented cells started to detach from ray parenchyma cells while most

of the cell lumina were still intact (Figure 2(c), orange dash lines). After 12 h of treatment, some cell lumina were fractured as a result of partial removal of lignin and hemicellulose (Figure 2(d)). Further decomposition of the thin cell walls was observed after 24 h: an increasing number of cell walls was fractured (marked in Figure 2(e) with a yellow dash frame), forming pores with diameters around 100 μm , larger than the cell lumina in native wood. The cell walls were completely destroyed after 48 h, due to further removal of lignin and hemicelluloses. As shown in Figure 2(f), fractured thin cell walls tend to be released during the freeze-drying process, resulting in a layered structure with relatively large spaces, and thus enhanced compressibility. The effects of the chemical treatment with a mixture of acetic acid and hydrogen peroxide on balsa wood can be summarized in three steps, comprising cell separation along rays followed by breakage of cell walls and eventual release of broken segments.

We also investigated the influence of the delignification approach on other wood species, including soft- and hardwoods. Figure S3(a), (b), (c), (d) shows the original microstructure before treatment of basswood, spruce, white pine and poplar, respectively. All these wood species have thicker cell walls when compared to balsa wood. After 48 h chemical treatment using the mixture of acetic acid and hydrogen peroxide followed by a freeze-drying step, these wood species did not show the lamellar structure found in balsa wood. As highlighted with yellow frames, some regions in the wood structure split along both horizontal and vertical directions, leading to a destruction of bulk wood due to total separation of cells (Figure S3(e), (f), (g) and (h)). Even though the delignification approach was the same, the structures produced by these wood species were dramatically different compared to those obtained with balsa wood. This may be related to the different thicknesses of cell walls. Balsa wood consists predominantly of thin-walled axial parenchyma (approximately 74%) and only by 4% of fibers,³⁸ while the other wood species have no or very little axial parenchyma

content.³⁹ It seems that all the investigated wood species split along the rays during the delignification process. However, the thin cell walls of balsa wood were more easily broken in the subsequent treatment while the delignification of the other wood species resulted in the separation of the cells, due to thicker and more stable cell walls. Hence, the approach of fabricating a lamellar sheet structure facilitating high compressibility by delignification with acetic acid and hydrogen peroxide seems to be limited to wood with a high content of thin-walled cells, like those found in balsa wood.

The wood weight loss as a function of time after chemical treatment is illustrated in Figure 2(g). The weight loss increased from 13.23% to 28.50%, 42.37%, 54.11% and 59.66% when the treatment time was increased from 3 h to 6 h, 12 h, 24 h and 48 h, respectively. X-ray diffraction (XRD) experiments were performed to study the cellulose in native wood and in the wood sponge after 48 h treatment. Characteristic diffraction peaks at 14.8° (1-10), 16.5° (110), and 22.5° (200) were observed for both native wood and the wood sponge (Figure 2(h)), indicating that cellulose is in its I form.²⁹

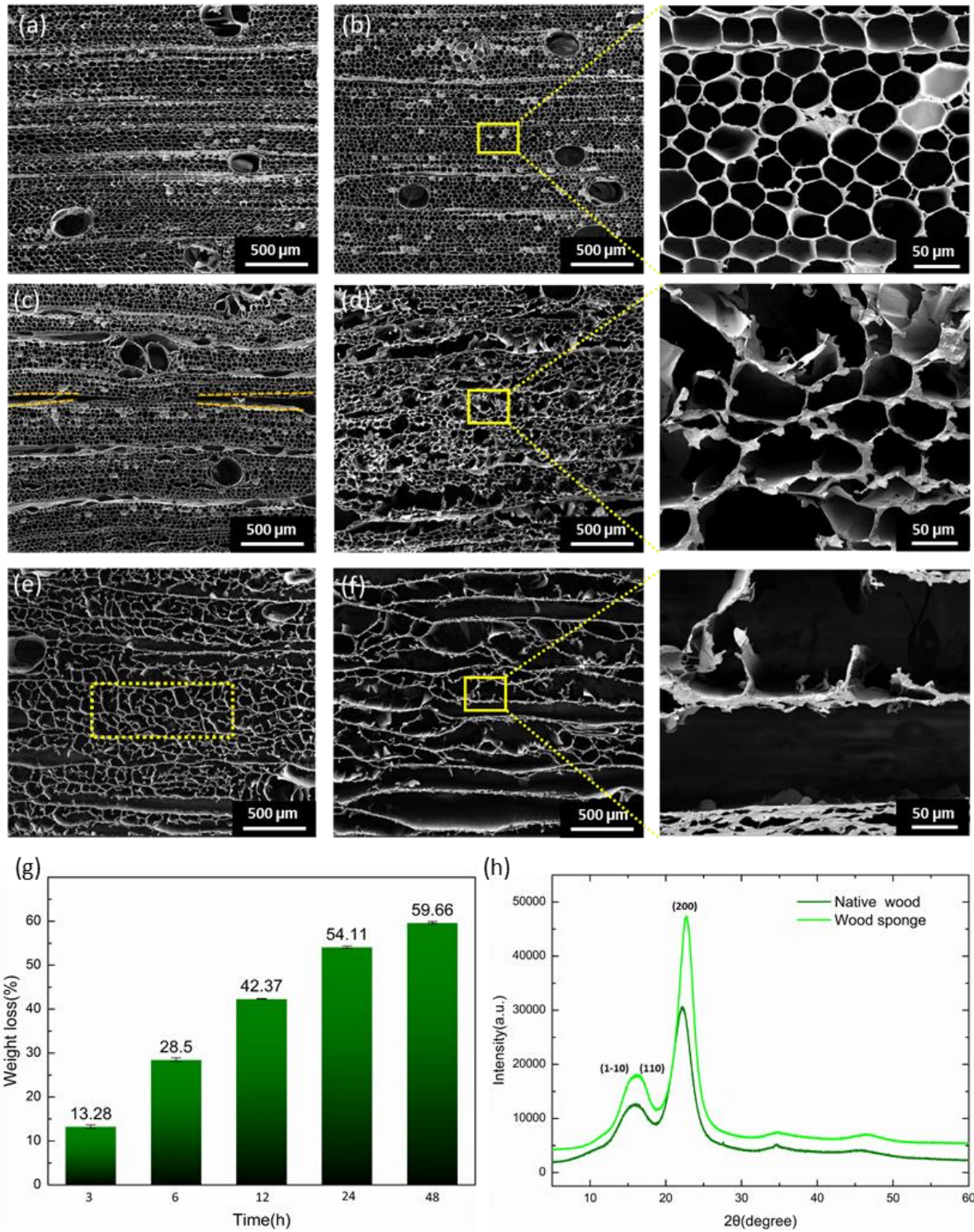


Figure 2. SEM images of delignification process of balsa wood (transverse sections) over time for (a) native wood, (b) 3 h treatment (at low and high magnitudes, respectively), (c) 6 h treatment, (d) 12 h treatment (at low and high magnitudes, respectively), (e) 24 h treatment, (f) 48 h treatment (at low and high magnitudes, respectively). (g) Changes of weight loss caused by chemical treatment over time. Error bars indicate standard deviations for five data points. (h) XRD patterns of native wood and wood sponge after 48 h treatment.

The mechanical properties of native balsa wood and of the wood sponge have been evaluated by performing multiple compression measurements in tangential direction. As shown in Figure 3(a) and S4, the wood sponge has a much higher compressibility compared to the rigid native wood. The application of a small stress of 13.3 kPa (≈ 3 N force), resulted in a strain of about 0.35% for the native wood and in a much higher strain of 45.83% for the wood sponge, corresponding to a 130-fold compressibility increase. The stress (σ)–strain (ϵ) curves obtained by applying different compressive stresses (4.4 kPa, 13.3 kPa, and 22.2 kPa) to the wood sponge are shown in Figure 3(b). Three distinct regions can be observed.⁴⁰⁻⁴² In the first region, a linear compression with strain below 20% is indicative of an liner- elastic deformation. A subsequent plateau, with a strain in the range of 20% to 30%, maybe related to the folding of cell segments. The stress increases sharply when the strain is beyond 30%, indicating increasing compaction of the sponge. The strain decrease to zero after unloading shows that the wood sponge was reversibly deformed and can completely recover to the original state after the release of the stress without plastic deformation (see also Figure S4). Figure 3(c) displays the cyclic stress–strain curves at a higher constant stress of 13.3 kPa used to evaluate the mechanical stability of the wood sponge. Small plastic deformations were observed after 50 loading-unloading cycles, indicating the good stability of the wood sponge. This feature can be further demonstrated by calculating the energy dissipation per cycle. As shown in Figure 3(d), the energy loss coefficient decreases from 0.47 (cycle 1) to 0.31 (cycle 50), which is relatively low compared to other reported aerogel materials with high compressibility.⁴³⁻⁴⁶ The excellent mechanical properties of the wood sponge, including its low energy loss coefficient and reversibility up to a strain of 51%, make it highly suitable for its application in piezoelectric nanogenerators.

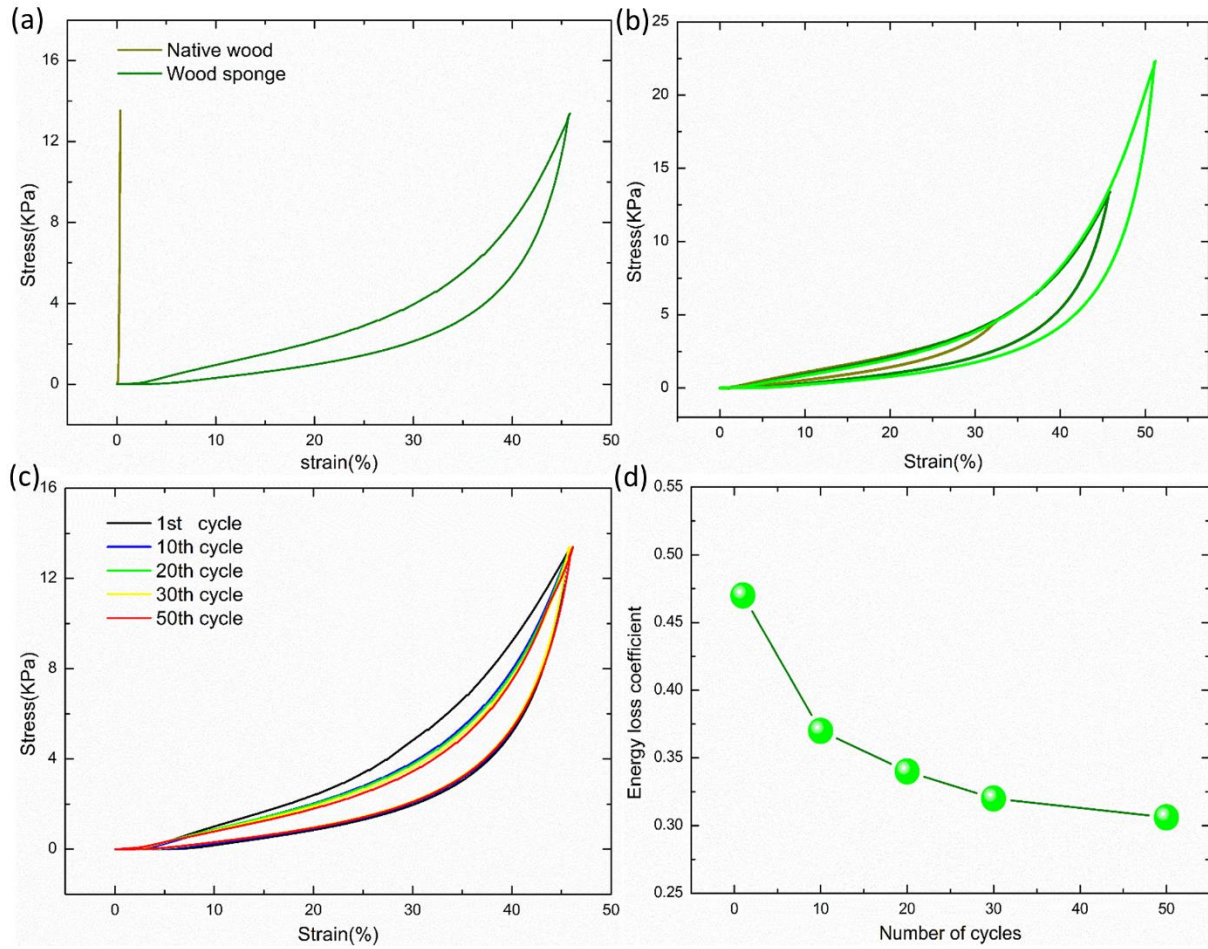


Figure 3. Results of multiple compression measurements in tangential direction. **(a)** Stress–strain curves of the native wood and wood sponge. **(b)** Stress–strain curves of the wood sponge under tangential compression with different maximum stress of 4.4 kPa, 13.3 kPa, and 22.2 kPa, respectively. **(c)** Stress–strain curves of the wood sponge under cyclic compression at a constant stress of 13.3 KPa. **(d)** Energy loss coefficient of the wood sponge during different cycles derived from the stress–strain curves in **(c)**.

When this wood sponge is compressed, electric charges are generated thanks to intrinsic piezoelectric behavior of crystalline cellulose. The piezoelectric output of both native balsa wood and wood sponge was measured by an electrometer (Keithley 6514). As shown in Figure 4(a), the native wood can only generate open-circuit voltage of 0.0081 V under a constant stress of 13.3 kPa. The corresponding short-circuit current was as small as 0.089 nA with heavy noise (Figure 4(b)). In contrast, the wood sponge shows a sharp improvement in voltage output (over 85 times), increasing up to 0.69 V (Figure 4(c)). A maximum short-circuit current of 7.1 nA was generated by the wood sponge, two orders of magnitude higher

than native wood, similar to voltage output. (Figure 4(d)). A long-term cyclic compressive loading/unloading test was performed to confirm the mechanical durability of the wood sponge under a constant stress of 13.3 kPa. As shown in Figure S5, the output voltage was maintained at approx. 0.63 V with minor fluctuations for up to 600 cycles with only a slight decline in the first 50 cycles, indicating a good stability. Figure S6 shows the resistance-dependent power density of the device: it reached a maximum value for a load resistance of 80 M Ω , corresponding to a peak power density of 0.6 nW/cm². Furthermore, the influence of the applied stress on the electrical output was studied. As shown in Figure 4(e) and (f), higher stresses resulted in both higher voltage and current, of 0.84 V and 8.2 nA respectively.

From the literature,²⁶ it is known that the piezoelectric effect in wood results from the mechanical deformation of crystalline cellulose, which unit cell is similar to monoclinic symmetry class 2 (where 2 is the two-fold symmetry axis). The enhanced deformation of a macroscopic wood sponge should induce higher displacement of cellulose crystals as a result of enhanced cell distortion during compression, and thus should lead to an increased electrical output. When the two-fold symmetry axis of the crystal lattice (longitudinal axis of the molecules) is parallel to z-axis, the piezoelectric tensor for this crystal can be written as:

$$\begin{array}{cccccc} 0 & 0 & 0 & d_{14} & d_{15} & 0 \\ 0 & 0 & 0 & d_{24} & d_{25} & 0 \\ d_{31} & d_{32} & d_{33} & 0 & 0 & d_{36} \end{array}$$

According to theory, eight piezoelectric moduli should exist in wood, including d_{14} , d_{15} , d_{24} , d_{25} , d_{13} , d_{32} , d_{33} , and d_{36} .²⁵ However, previous reports on the piezoelectric effect in wood focused on the d_{14} and d_{25} moduli, which require shear stress to be activated. We hypothesize that the electrical output produced by the wood sponge could also benefit from the synergistic contribution of different piezoelectric moduli, such as d_{25} (as it is known that the fiber

misalignment in balsa wood leads to the formation of shear stresses under mechanical compression^{47, 48}) and d_{32} (which is induced by compression force and has been recently found in native wood²⁸). However, to measure these moduli and the piezoelectric coefficient of our wood sponge remains an open challenge. Piezoresponse force microscopy (PFM)^{49, 50} has been demonstrated in previous studies as a powerful tool to measure the piezoelectric coefficient of pure cellulose films or cellulose composites, but has not yet been tested on a complex matrix such as our wood sponge. Hence, further investigations are needed to gain a better understanding of the piezoelectric properties of the wood sponge nanogenerator. In addition, comparison of the piezoelectric constant of the wood sponge with other piezoelectric materials is not straightforward. We can only estimate that the piezoelectric constant of wood sponge should be smaller than more conventional, high-performance piezoelectric materials such as barium titanate or PZT.

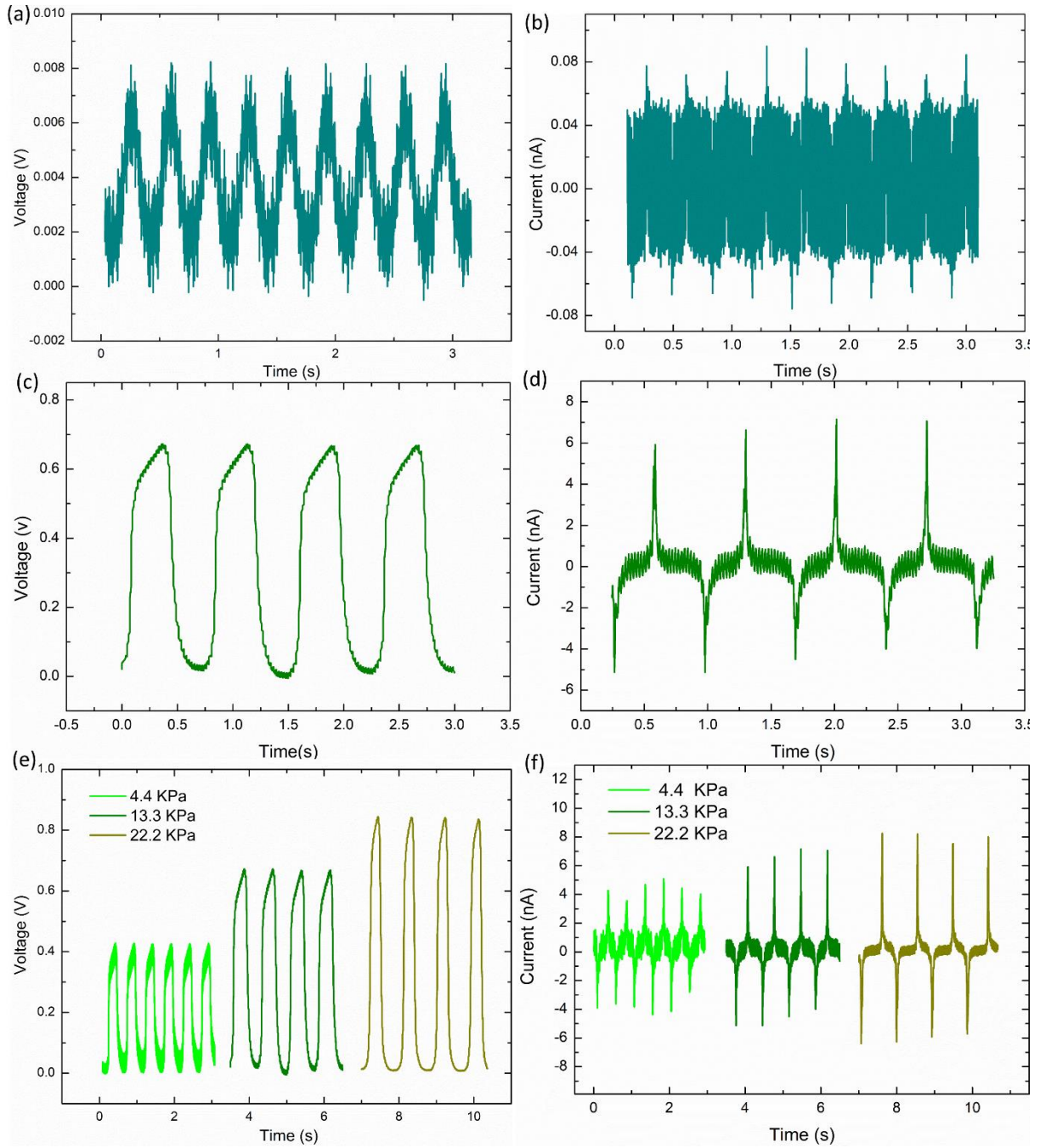


Figure 4. Comparison of the piezoelectric outputs (voltage and current) of native wood and of the resulting wood sponge. **(a)** Output voltage of the native wood. **(b)** Current output of native wood. **(c)** Voltage of the wood sponge under a constant stress of 13.3 kPa. **(d)** Output current of the wood sponge. Output voltage **(e)** and current **(f)** of the wood sponge under compression with different maximum stress of 4.4 kPa, 13.3 kPa, and 22.2 kPa.

Its sensitivity to mechanical deformation makes this lightweight, biocompatible and biodegradable wood nanogenerator well-suited for wearable sensing applications, converting

various human motions into electrical signals. As illustrated in Figure 5(a), this nanogenerator can be directly attached to different body parts for detecting the associated physiological signals. Moreover, this nanogenerator can be upscaled and incorporated into wood furniture, such as a wooden table or floor, to endow the building interior with energy harvest function. (Figure 5 (b)). Electricity can then be produced through a variety of human actions, such as tapping on the table or walking on the floor. Figure 5(c)-(g) displays a series of examples for practical applications of both wearable sensing and built-in energy supplies. When tapping on the wood nanogenerator with a finger, a voltage (around 0.06 V) is generated as shown in Figure 5(c). Figure 5(d) displays the voltage curve measured for our nanogenerator attached onto a knuckle, which precisely reflects the bending of the finger (inset in Figure 5(d) shows photographs of this motion).

To demonstrate the potential for upscaling as efficient energy supply, we fabricated a larger-scale demonstrator made of 30 wood sponges connected in parallel. This upscaled nanogenerator demonstrator can produce a current of up to 205 nA, as shown in Figure S7. (the slight loss of output current can be attributed to leakage of the circuit.) As illustrated in Figure 5(e), two pieces of copper foil with a size of 90 mm x 75 mm were attached onto the radial sections of our wood sponges, which were then covered with two pieces of 1 mm-thick wood veneer. Various portable low-power electronics, such as light emitting diodes (LEDs) and liquid crystal display (LCD) screens, were electrically connected. A small LED could be switched on by tipping on the demonstrator (Figure S8). Figure 5(f) and (g) illustrate the application potential for powering a monochromatic display device with LCD screen by walking on the demonstrator. For a transition towards bio-economy, it is of utmost importance to develop innovative electrical devices that are biodegradable and do not cause environmental pollution. To demonstrate the environmental-friendliness of our generator, after peeling off the copper foil, we inoculated the bare wood sponge with a common

cellulose-degrading fungi strain (*Coniophora puteana*). Figure S9 shows a sequence of images of the fungi-inoculated wood sponge taken after 6 weeks, 8 weeks and 10 weeks, respectively. The complete loss of the original shape and substantial size reduction confirm the successful biodegradation of the wood sponge.

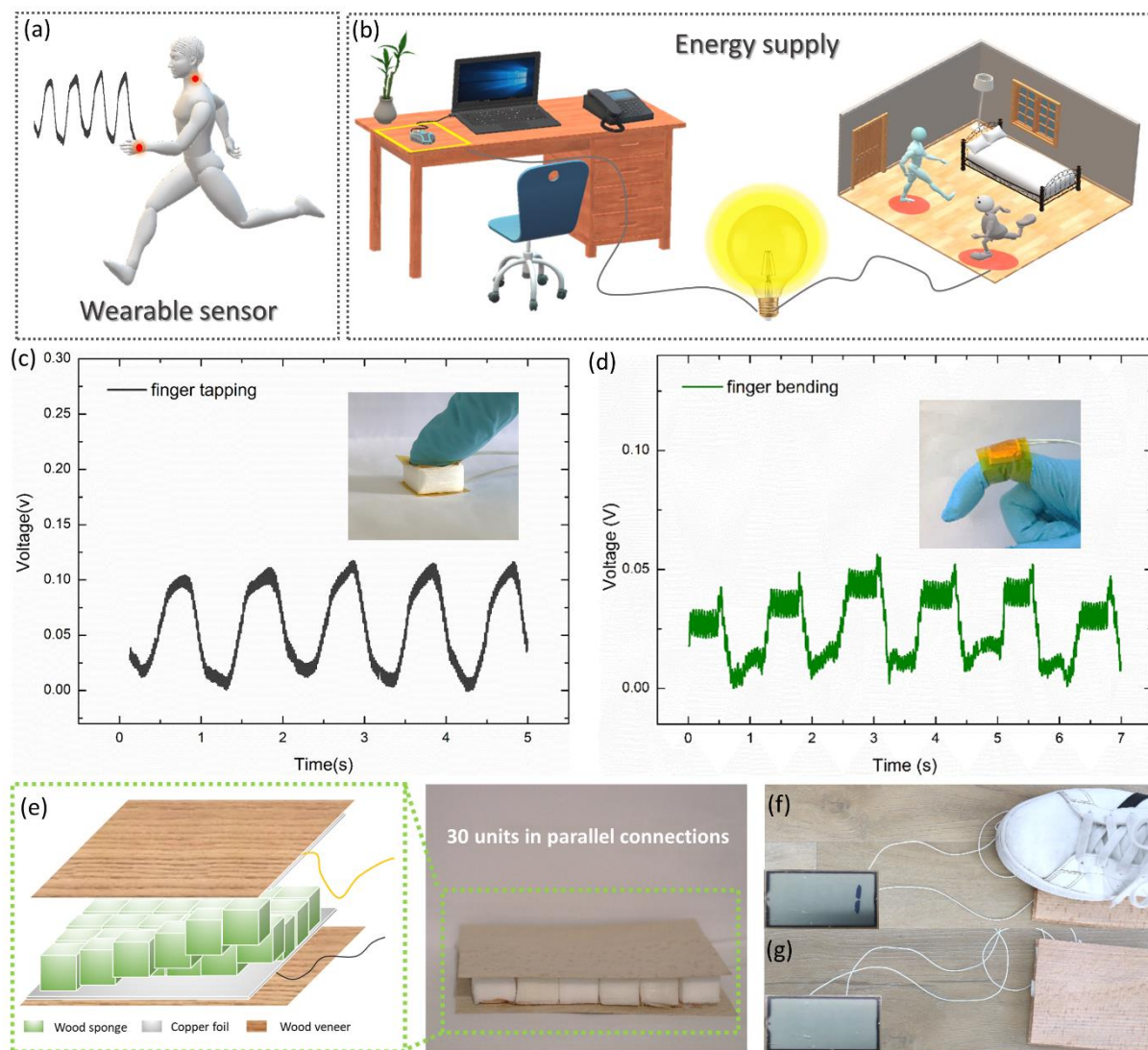


Figure 5. Proof-of-concept applications of our wood sponge nanogenerator. **(a)** Schematic illustration showing the application as wearable sensor. **(b)** Schematic illustration of applications for energy supply. **(c)** Example of movement sensing: finger tapping. **(d)** Example of movement sensing: finger bending. **(e)** Schematic illustration of upscaling by assembly of multiple wood sponges. **(f)** and **(g)** Demonstration of the resulting piezoelectric wooden floor prototype, able to power a commercial LCD screen (Inset pictures) when pressed with a foot.

CONCLUSION

We have reported here a low-cost, biodegradable, biocompatible and highly efficient piezoelectric nanogenerator based on a wood sponge, fabricated by a simple delignification process. Our wood sponge piezoelectric generator ($15 \times 15 \times 14 \text{ mm}^3$, longitudinal \times radial \times tangential) was able to generate an instantaneous voltage of up to 0.69 V and a current of 7.1 nA upon the application of a relatively small stress of 13.3 kPa, with an 85-fold increase in performance compared to native wood thanks to the increased compressibility. Our approach indicates the importance of increased compressibility of bulk wood materials towards effectively improving their piezoelectric output. We demonstrated the use of the piezoelectric nanogenerator as a smart pressure sensor, attaching it to a finger to monitor human motions through the corresponding electrical signals. Moreover, we were able to significantly increase the maximum output current ($\approx 205 \text{ nA}$) by connecting 30 wood sponges in parallel to each other, making a demonstrator suitable for wooden tables or floors. By tapping or walking on the demonstrator, a commercial LED or LCD screen could be turned-on, indicating potential application as power supply in smart buildings. Because the active element of the generator is a plain wood sponge, we demonstrated that it can be gradually degraded by common fungi in a few weeks. Our results show the potential application of wood sponges in the field of sustainable and renewable energy sources, wearable sensors for monitoring human motions, as well as environmental protection by electronic waste reduction.

METHODS

Wood sponge preparation

Wood samples of *Ochroma pyramidale* Cav. ex Lam. (Balsa) were cut into cubes of $15T \times 15R \times 15L \text{ mm}^3$. The initial weight was recorded after oven-drying the samples at 103°C for 24 h. The wood samples were delignified using a mixture of 400 mL acetic acid ($\geq 99.7\%$, Sigma-Aldrich) and 400 mL hydrogen peroxide (30%, Sigma-Aldrich) at 85°C for up to 48

h. Then, the delignified samples were washed in deionized water for 48 h to remove the chemicals. Finally, the samples were freeze-dried at $-40\text{ }^{\circ}\text{C}$ for 48 h, resulting in highly porous wood sponges. Five replicates per batch were made. The final weight was recorded after drying the samples in the oven at $103\text{ }^{\circ}\text{C}$ for 24 h and the weight loss was calculated as percentage of the initial weight.

Characterization

The obtained wood sponge was characterized by various techniques. The microstructure was studied by field emission scanning electron microscopy (FE-SEM) (FEI Quanta 200F) after coating Pt/Pd nanoparticles on the surface using the coating device CCU-010 Metal Sputter Coater Safematic HPM A53. The mechanical properties in radial/tangential compression were evaluated with an universal mechanical testing machine (Shimadzu AGS-X, Japan), equipped with a 100 N load cell. Fourier-transform infrared spectroscopy (FTIR) (Bruker Tensor 27) was performed over a range of $400\text{--}4000\text{ cm}^{-1}$ to analyse the changes in composition before and after the chemical delignification treatment. The crystallinity of cellulose in the wood sponge was studied by X-ray diffraction (Panalytical X'Pert PRO MPD) using Cu K α radiation ($\lambda = 1.5406\text{ \AA}$). To measure the piezoelectric output of the samples, a Keithley 6514 electrometer was used. A linear motor (PL01-28x500/420) was used to apply a fixed pressure to compress the samples with a 50 N load cell to monitor the pressure. Furthermore, the effective power density of our device was calculated by measuring the voltage output as a function of the external load resistors varying from 1 to $120\text{ M}\Omega$ under a stress of 13.3 MPa .

Assembly of the large-scale demonstrator

An up-scaled demonstrator was made combining 30 wood sponges electrically connected in parallel. Then, two pieces of copper foil with a size of $90\text{ mm} \times 75\text{ mm}$ were attached onto

the radial sections of the wood sponges, which were then covered with two pieces of 1 mm-thick wood veneer.

Biodegradation of the wood sponge

The bare wood sponges were sterilized with ethylene oxide (Sigma-Aldrich, Buchs, Switzerland) and then placed into Kolle culture flasks containing freshly inoculated *C. puteana* growing on 75 mL of 4% Malt Extract Agar (Oxoid, Platern, Switzerland). Three replicates for each incubation period (6, 8, 10 weeks) were studied. All cultures were maintained in the dark at 22°C and 70% relative humidity. After the chosen incubation time, the samples were carefully removed, the fungal biomass was removed from the surface and the shape of the wood sponge samples was recorded with a digital color camera (Nikon Coolpix 990).

ASSOCIATED CONTENT

Supporting Information. The Supporting Information is available free of charge at (link: <https://pubs.acs.org/doi/xx/acsnano.xx>.)

Figures S1–S9 provide SEM images of a tangential-longitudinal section of the wood sponge; SEM images of transverse sections of balsa wood samples before and after chemical delignification; SEM images of transverse sections of different wood species before and after chemical delignification; photographs of the wood sponge showing its high and reversible compressibility; output voltage of a single wood sponge subjected to 600 cyclic compression cycles; the variation of output voltage and power density with resistance; output voltage of the large-scale generator (30 wood sponges connected parallel to each other); wooden table for powering a commercial LED in the dark; Images showing wood sponges after treatment with the cellulose-degrading fungus *Coniophora puteana* for different times. (PDF)

AUTHOR CONTRIBUTIONS

The manuscript was written through contributions of all authors. All authors have given approval to the final version of the manuscript.

The authors declare no competing financial interest.

ACKNOWLEDGMENT

There is no funding source to declare. We are grateful to Thomas Schnider for cutting the balsa wood cubes.

REFERENCES

1. Wang, Z. L.; Song, J. H. Piezoelectric Nanogenerators Based on Zinc Oxide Nanowire Arrays. *Science* **2006**, *312*, 242-246.
2. Yang, R. S.; Qin, Y.; Dai, L. M.; Wang, Z. L. Power Generation with Laterally Packaged Piezoelectric Fine Wires. *Nat. Nanotechnol.* **2009**, *4*, 34-39.
3. Midilli, A.; Ay, M.; Dincer, I.; Rosen, M. A. On Hydrogen and Hydrogen Energy Strategies I: Current Status and Needs. *Renew. Sust. Energ. Rev.* **2005**, *9*, 255-271.
4. Ball, J. M.; Lee, M. M.; Hey, A.; Snaith, H. J. Low-Temperature Processed Meso-Superstructured to Thin-Film Perovskite Solar Cells. *Energ. Environ. Sci.* **2013**, *6*, 1739-1743.
5. Breton, S. P.; Moe, G. Status, Plans and Technologies for Offshore Wind Turbines in Europe and North America. *Renew. Energ.* **2009**, *34*, 646-654.
6. Chen, B.; Yang, Y.; Wang, Z. L. Scavenging Wind Energy by Triboelectric Nanogenerators. *Adv. Energy Mater.* **2018**, *8*, 1702649.

7. Li, X. H.; Lin, Z. H.; Cheng, G.; Wen, X. N.; Liu, Y.; Niu, S. M.; Wang, Z. L. 3D Fiber-Based Hybrid Nanogenerator for Energy Harvesting and as a Self-Powered Pressure Sensor. *ACS Nano* **2014**, *8*, 10674-10681.
8. Sun, J. G.; Yang, T. N.; Kuo, I. S.; Wu, J. M.; Wang, C. Y.; Chen, L. J. A Leaf-Molded Transparent Triboelectric Nanogenerator for Smart Multifunctional Applications. *Nano Energy* **2017**, *32*, 180-186.
9. Beeby, S. P.; Torah, R. N.; Tudor, M. J.; Glynne-Jones, P.; O'Donnell, T.; Saha, C. R.; Roy, S. A Micro Electromagnetic Generator for Vibration Energy Harvesting. *J. Micromech. Microeng.* **2007**, *17*, 1257-1265.
10. Lee, S. H.; Jeong, C. K.; Hwang, G. T.; Lee, K. J. Self-Powered Flexible Inorganic Electronic System. *Nano Energy* **2015**, *14*, 111-125.
11. Sun, J. G.; Yang, T. N.; Wang, C. Y.; Chen, L. J. A Flexible Transparent One-Structure Tribo-Piezo-Pyroelectric Hybrid Energy Generator Based on Bio-Inspired Silver Nanowires Network for Biomechanical Energy Harvesting and Physiological Monitoring. *Nano Energy* **2018**, *48*, 383-390.
12. Wang, Z. L. Triboelectric Nanogenerators as New Energy Technology for Self-Powered Systems and as Active Mechanical and Chemical Sensors. *ACS Nano* **2013**, *7*, 9533-9557.
13. Zhang, X. S.; Han, M. D.; Meng, B.; Zhang, H. X. High Performance Triboelectric Nanogenerators Based on Large-Scale Mass-Fabrication Technologies. *Nano Energy* **2015**, *11*, 304-322.

14. Zhu, M. L.; Shi, Q. F.; He, T. Y. Y.; Yi, Z. R.; Ma, Y. M.; Yang, B.; Chen, T.; Lee, C. Self-Powered and Self-Functional Cotton Sock Using Piezoelectric and Triboelectric Hybrid Mechanism for Healthcare and Sports Monitoring. *ACS Nano* **2019**, *13*, 1940-1952.
15. Qiu, C. K.; Wu, F.; Lee, C.; Yuce, M. R. Self-Powered Control Interface Based on Gray Code with Hybrid Triboelectric and Photovoltaics Energy Harvesting for IoT Smart Home and Access Control Applications. *Nano Energy* **2020**, *70*, 104456.
16. Jiang, W.; Li, H.; Liu, Z.; Li, Z.; Tian, J.; Shi, B.; Zou, Y.; Ouyang, H.; Zhao, C.; Zhao, L.; Sun, R.; Zheng, H.; Fan, Y.; Wang, Z. L.; Li, Z. Fully Bioabsorbable Natural-Materials-Based Triboelectric Nanogenerators. *Adv. Mater.* **2018**, *30*, e1801895.
17. He, T.; Wang, H.; Wang, J.; Tian, X.; Wen, F.; Shi, Q.; Ho, J. S.; Lee, C. Self-Sustainable Wearable Textile Nano-Energy Nano-System (NENS) for Next-Generation Healthcare Applications. *Adv. Sci.* **2019**, *6*, 1901437.
18. Saifei Haoa, J. J., Yandong Chen, Zhong Lin Wang, Xia Cao. Natural Wood-Based Triboelectric Nanogenerator as Self-Powered Sensing for Smart Homes and Floors. *Nano Energy* **2020**, *75*, 104957.
19. Wang, X. D.; Song, J. H.; Liu, J.; Wang, Z. L. Direct-Current Nanogenerator Driven by Ultrasonic Waves. *Science* **2007**, *316*, 102-105.
20. Mitcheson, P. D.; Miao, P.; Stark, B. H.; Yeatman, E. M.; Holmes, A. S.; Green, T. C. MEMS Electrostatic Micropower Generator for Low Frequency Operation. *Sensors Actuators A-Phys.* **2004**, *115*, 523-529.
21. Karan, S. K.; Mandal, D.; Khatua, B. B. Self-Powered Flexible Fe-Doped RGO/PVDF Nanocomposite: An Excellent Material for a Piezoelectric Energy Harvester. *Nanoscale* **2015**, *7*, 10655-10666.

22. Yan, J.; Jeong, Y. G. High Performance Flexible Piezoelectric Nanogenerators Based on BaTiO₃ Nanofibers in Different Alignment Modes. *ACS. Appl. Mater. Inter.* **2016**, *8*, 15700-15709.
23. Park, K. I.; Xu, S.; Liu, Y.; Hwang, G. T.; Kang, S. J. L.; Wang, Z. L.; Lee, K. J. Piezoelectric BaTiO₃ Thin Film Nanogenerator on Plastic Substrates. *Nano Lett.* **2010**, *10*, 4939-4943.
24. Karan, S. K.; Maiti, S.; Kwon, O.; Paria, S.; Maitra, A.; Si, S. K.; Kim, Y.; Kim, J. K.; Khatua, B. B. Nature Driven Spider Silk as High Energy Conversion Efficient Bio-Piezoelectric Nanogenerator. *Nano Energy* **2018**, *49*, 655-666.
25. Fukada, E. Piezoelectricity of Wood. *J. Phys. Soc. Jpn.* **1955**, *10*, 149-154.
26. Fukada, E. Piezoelectricity as a Fundamental Property of Wood. *Holzforschung* **1967**, *21*, 186-189.
27. Shamos, M. H.; Lavine, L. S. Piezoelectricity as a Fundamental Property of Biological Tissues. *Nature* **1967**, *213*, 267-269.
28. Hirai, N.; Sobue, N.; Date, M. New Piezoelectric Moduli of Wood: d(31) and d(32). *J. Wood Sci.* **2011**, *57*, 1-6.
29. Guan, H.; Cheng, Z. Y.; Wang, X. Q. Highly Compressible Wood Sponges with a Spring-Like Lamellar Structure as Effective and Reusable Oil Absorbents. *ACS Nano* **2018**, *12*, 10365-10373.
30. Chen, C. J.; Song, J. W.; Zhu, S. Z.; Li, Y. J.; Kuang, Y. D.; Wan, J. Y.; Kirsch, D.; Xu, L. S.; Wang, Y. B.; Gao, T. T.; Wang, Y. L.; Huang, H.; Gan, W. T.; Gong, A.; Li, T.; Xie, J.; Hu, L. B. Scalable and Sustainable Approach toward Highly Compressible, Anisotropic, Lamellar Carbon Sponge. *Chem* **2018**, *4*, 544-554.

31. Frey, M.; Widner, D.; Segmehl, J. S.; Casdorff, K.; Keplinger, T.; Burgert, I. Delignified and Densified Cellulose Bulk Materials with Excellent Tensile Properties for Sustainable Engineering. *ACS Appl. Mater. Inter.* **2018**, *10*, 5030-5037.
32. Lee, C.; Tarbutton, J. A. Electric Poling-Assisted Additive Manufacturing Process for PVDF Polymer-Based Piezoelectric Device Applications. *Smart Mater. Struct.* **2014**, *23*, 095044.
33. Luo, J. J.; Wang, Z. M.; Xu, L.; Wang, A. C.; Han, K.; Jiang, T.; Lai, Q. S.; Bai, Y.; Tang, W.; Fan, F. R.; Wang, Z. L. Flexible and Durable Wood-Based Triboelectric Nanogenerators for Self-Powered Sensing in Athletic Big Data Analytics. *Nat. Commun.* **2019**, *10*, 5147.
34. Shi, K. M.; Huang, X. Y.; Sun, B.; Wu, Z. Y.; He, J. L.; Jiang, P. K. Cellulose/BaTiO₃ Aerogel Paper Based Flexible Piezoelectric Nanogenerators and the Electric Coupling with Triboelectricity. *Nano Energy* **2019**, *57*, 450-458.
35. Kim, I.; Jeon, H.; Kim, D.; You, J.; Kim, D. All-In-One Cellulose Based Triboelectric Nanogenerator for Electronic Paper Using Simple Filtration Process. *Nano Energy* **2018**, *53*, 975-981.
36. Chen, C. J.; Li, Y. J.; Song, J. W.; Yang, Z.; Kuang, Y.; Hitz, E.; Jia, C.; Gong, A.; Jiang, F.; Zhu, J. Y.; Yang, B.; Xie, J.; Hu, L. B. Highly Flexible and Efficient Solar Steam Generation Device. *Adv. Mater.* **2017**, *29*, 1701756.
37. Ciriminna, R.; Albanese, L.; Meneguzzo, F.; Pagliaro, M. Hydrogen Peroxide: a Key Chemical for Today's Sustainable Development. *Chemsuschem.* **2016**, *9*, 3374-3381.

38. Follrich, J.; Hora, M.; Muller, U.; Teischinger, A.; Gindl, W. Adhesive Bond Strength of End Grain Joints in Balsa Wood with Different Density. *Wood Res-Slovakia*. **2010**, *55*, 21-31.
39. Stobbe, H.; Schmitt, U.; Eckstein, D.; Dujesiefken, D. Developmental Stages and Fine Structure of Surface Callus Formed after Debarking of Living Lime Trees (*Tilia sp.*). *Ann. Bot-London* **2002**, *89*, 773-782.
40. Hu, H.; Zhao, Z. B.; Wan, W. B.; Gogotsi, Y.; Qiu, J. S. Ultralight and Highly Compressible Graphene Aerogels. *Adv. Mater.* **2013**, *25*, 2219-2223.
41. Wu, Z. Y.; Li, C.; Liang, H. W.; Chen, J. F.; Yu, S. H. Ultralight, Flexible, and Fire-Resistant Carbon Nanofiber Aerogels from Bacterial Cellulose. *Angew. Chem. Int. Ed.* **2013**, *52*, 2925-2929.
42. Song, J. W.; Chen, C. J.; Yang, Z.; Kuang, Y. D.; Li, T.; Li, Y. J.; Huang, H.; Kierzewski, I.; Liu, B. Y.; He, S. M.; Gao, T. T.; Yuruker, S. U.; Gong, A.; Yang, B.; Hu, L. B. Highly Compressible, Anisotropic Aerogel with Aligned Cellulose Nanofibers. *ACS Nano* **2018**, *12*, 140-147.
43. Sun, H. Y.; Xu, Z.; Gao, C. Multifunctional, Ultra-Flyweight, Synergistically Assembled Carbon Aerogels. *Adv. Mater.* **2013**, *25*, 2554-2560.
44. Zhu, C.; Han, T. Y. J.; Duoss, E. B.; Golobic, A. M.; Kuntz, J. D.; Spadaccini, C. M.; Worsley, M. A. Highly Compressible 3D Periodic Graphene Aerogel Microlattices. *Nat. Commun.* **2015**, *6*, 6962.
45. Li, Y. R.; Chen, J.; Huang, L.; Li, C.; Hong, J. D.; Shi, G. Q. Highly Compressible Macroporous Graphene Monoliths via an Improved Hydrothermal Process. *Adv. Mater.* **2014**, *26*, 4789-4793.

46. Qiu, L.; Liu, J. Z.; Chang, S. L. Y.; Wu, Y. Z.; Li, D. Biomimetic Superelastic Graphene-Based Cellular Monoliths. *Nat. Commun.* **2012**, *3*, 1241.
47. Vural, M.; Ravichandran, G. Microstructural Aspects and Modeling of Failure in Naturally Occurring Porous Composites. *Mech. Mater.* **2003**, *35*, 523-536.
48. Da Silva, A.; Kyriakides, S. Compressive Response and Failure of Balsa Wood. *Int. J. Solids Struct.* **2007**, *44*, 8685-8717.
49. Lindong Zhai, H. C. K., Jung Woong Kim, and Jaehwan Kim, Alignment Effect on the Piezoelectric Properties of Ultrathin Cellulose Nanofiber Films. *ACS Appl. Bio. Mater.* **2020**, *7*, 4329-4334.
50. Calahorra, Y.; Datta, A.; Famelton, J.; Kam, D.; Shoseyov, O.; Kar-Narayan, S. Nanoscale Electromechanical Properties of Template-Assisted Hierarchical Self-Assembled Cellulose Nanofibers. *Nanoscale* **2018**, *10*, 16812-16821.

Table of Contents

